Microphase separation and the formation of ion conductivity channels in poly(ionic liquid)s: A coarse-grained molecular dynamics study

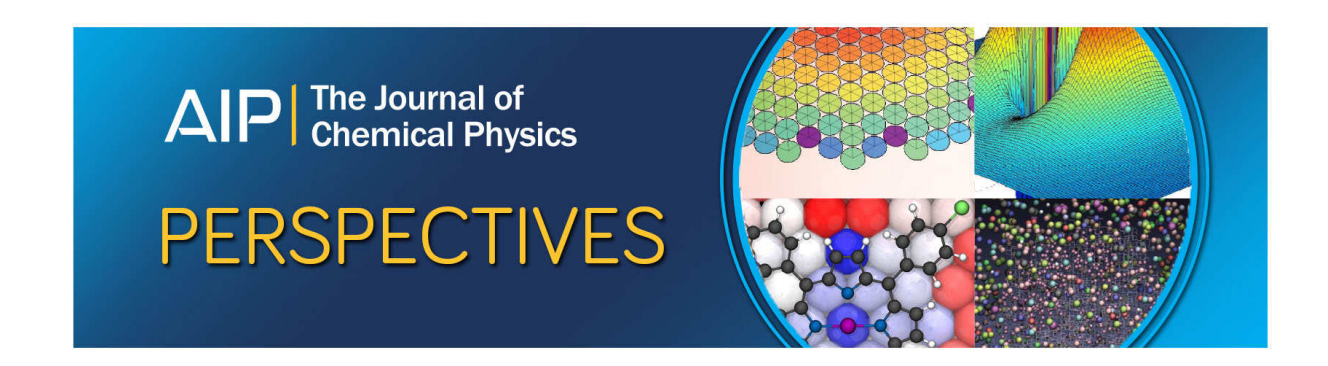
Alexander Weyman, Markus Bier, Christian Holm, and Jens Smiatek

Citation: The Journal of Chemical Physics 148, 193824 (2018);

View online: https://doi.org/10.1063/1.5016814

View Table of Contents: http://aip.scitation.org/toc/jcp/148/19

Published by the American Institute of Physics





Microphase separation and the formation of ion conductivity channels in poly(ionic liquid)s: A coarse-grained molecular dynamics study

Alexander Weyman, ^{1,2,a)} Markus Bier, ^{3,4,b)} Christian Holm, ^{1,c)} and Jens Smiatek ^{1,5,d)}

¹Institute for Computational Physics, University of Stuttgart, Allmandring 3, D-70569 Stuttgart, Germany

²ETH Zürich, Department of Materials, Leopold-Ruzicka-Weg 4, CH-8093 Zürich, Switzerland

³Max Planck Institute for Intelligent Systems, Heisenbergstrasse 3, D-70569 Stuttgart, Germany

⁴Institute for Theoretical Physics IV, University of Stuttgart, Pfaffenwaldring 57, D-70569 Stuttgart, Germany

⁵Helmholtz Institute Muenster (HIMS-IEK 12), Forschungszentrum Juelich, Corrensstrasse 46,

D-48149 Muenster, Germany

(Received 21 November 2017; accepted 29 January 2018; published online 14 February 2018)

We study generic properties of poly(ionic liquid)s (PILs) via coarse-grained molecular dynamics simulations in bulk solution and under confinement. The influence of different side chain lengths on the spatial properties of the PIL systems and on the ionic transport mechanism is investigated in detail. Our results reveal the formation of apolar and polar nanodomains with increasing side chain length in good agreement with previous results for molecular ionic liquids. The ion transport numbers are unaffected by the occurrence of these domains, and the corresponding values highlight the potential role of PILs as single-ion conductors in electrochemical devices. In contrast to bulk behavior, a pronounced formation of ion conductivity channels in confined systems is initiated in close vicinity to the boundaries. We observe higher ion conductivities in these channels for increasing PIL side chain lengths in comparison with bulk values and provide an explanation for this effect. The appearance of these domains points to an improved application of PILs in modern polymer electrolyte batteries. *Published by AIP Publishing*, https://doi.org/10.1063/1.5016814

I. INTRODUCTION

Polymerized ionic liquids (PILs) or poly(ionic liquid)s are a special class of polymers, based on the chemistry of ionic liquids, with beneficial properties such as pronounced electrochemical stability and high ionic conductivity. In contrast to molecular ionic liquids, either the organic cation or the organic anion is covalently bound to a polymer backbone, which minimizes leakage problems in technological applications and which promotes single ion transport. In more detail, the molecular units (monomers) of PILs are in part composed of organic ions such that these building units can also be called ionic liquid monomers (ILMs). As a further advantage, PILs conduct ions even in the absence of solvents, which is also beneficial for high temperature operation in modern electrochemical devices. Typical representatives of PILs are often based on dialkylimidazolium cations with their corresponding counterions as depicted in Fig. 1.

As a consequence of the organic ion group, PILs combine the benefits of ionic liquids with desirable properties of polymers and thus were discussed as potential conductive materials in many applications. Pioneering work was published nearly twenty years ago, when the properties of polymerized imidazolium cations and sulfonamide salts were first investigated by Ohno and Ito. Over the last years, several review articles 1,3-5 reported the progress from first generation PILs

mental understanding, a recent atomistic molecular dynamic

to new types of materials, which have thus formed the basis for entirely new fields of applications such as CO₂ storage and separation of CO₂ in PIL membranes.^{6–9} As the physico-

chemical properties of PILs strongly depend on the choice

of the mobile counterions (cf. Fig. 1), anion sensitive smart

materials in terms of switchable surfaces besides other applications were introduced, whose solubility, hydrophilicity, or

volume can be modified explicitly by anion exchange reac-

tions. Recently, PILs were also used as solvent sensors 10,11

and as tailor-made high performance polymer electrolytes in electrochemical devices. ^{1,12} On this occasion, PILs are usually

mixed with their ionic liquid analogues in order to improve the cyclability and long-term stability, to solve leakage prob-

lems in lithium ion batteries, ¹³ or to increase the electrode

surface area accessible to ionic liquid-based electrolytes in

supercapacitors.¹⁴ The observed high ionic conductivity in

PIL systems was attributed to low melting and low glass transition temperatures, ¹⁵ and recent effort in optimizing charge

transport mostly focused on the rheological stability of the

materials, ¹⁶ exchange of anion species, ¹⁷ or variations in the chemical composition. ^{18–22}

In contrast to the rising interest in applications, computational and theoretical studies of PILs were only sparsely performed. Thus, the molecular properties and the resulting spatial arrangement of the system are only known in some parts. Moreover, ion transport phenomena remain mostly unresolved, and it is not clear if typical properties of molecular ionic liquids, for instance the formation of apolar domains in terms of dialkylimidazolium based ionic liquids, can be also observed in PILs. ^{23,24} As a first step towards a more funda-

a)Electronic mail: alexander.weyman@mat.ethz.ch

b)bier@is.mpg.de

c)Electronic mail: holm@icp.uni-stuttgart.de

d)Electronic mail: smiatek@icp.uni-stuttgart.de

$$R = H \text{ or alkyl}$$
 $X = BF_4, PF_6, TFSI, CF_3SO_3, SCN, ...$

FIG. 1. Representative examples of dialkylimidazolium-based PILs with different side chain lengths. The selection of anions \mathbf{X}^- is made similar to Mecerreyes. 1

(MD) simulation study focused on the properties of bound and mobile counterions and the corresponding influence on the ion transport.²⁵

The close relationship between PILs and standard polyelectrolytes also motivates the use of coarse-grained models in order to study generic properties of the system at larger length and longer time scales. Previous simulation studies with coarse-grained models for polyelectrolytes already lead to the detection of pearl-necklace structures in poor solvents, ²⁶ size-dependent electrophoretic mobilities,²⁷ the study of coupled electroosmotic/electrophoretic effects in microchannels, ^{28,29} or the influence of locally varying dielectric permittivities on the conductivity of salty polyelectrolyte solutions.³⁰ In addition, further simple approaches for ionomers were also developed in order to study the properties of microphase separation and the corresponding charge transport in presence and in absence of external electric fields.^{31,32} Hence, coarsegrained models have proven their applicability, also for molecular ionic liquids, ^{33–36} and it can be expected that they can be also regarded as a versatile approach for the study of PIL systems.

In this article, we introduce a simple bead-spring model for coarse-grained poly(ionic liquid)s, which is suitable for the analysis of microphase separation effects³⁷ and the formation of ion conductivity channels in agreement with recent experimental results.^{38,39} Due to these reasons, we are confident that our simulation results will contribute to a deeper understanding of PIL systems and to a further optimization of these materials for the use in electrochemical devices.

The article is organized as follows. In Sec. II, we discuss the theoretical background for the analysis of our simulations. The computational details and the PIL bead-spring model are introduced in Sec. III. We present all simulation outcomes in Sec. IV, and we briefly conclude and summarize in Sec. V.

II. THEORETICAL BACKGROUND

The local composition of a PIL system at different length scales can be studied through partial structure factors, which were already established for molecular ionic liquid/water mixtures^{24,40} according to the relation^{41,42}

$$S_{ij}(q) = \frac{N_i}{N} \left(\delta_{ij} + \rho_j \int_0^\infty \frac{\sin(qr)}{qr} [g_{ij}(r) - 1] 4\pi r^2 dr \right), \quad (1)$$

with the wave number q, the Kronecker delta δ_{ij} , the bulk number density $\rho_j = N_j/V$ of species j with the number of particles N_j in volume V, the total number of particles N, and the radial distribution function $g_{ij}(r)$ between the considered species. In the limit $q \to 0$, it was shown⁴² that the partial structure factor [Eq. (1)] reduces to

$$S_{ij}(0) \approx \frac{N_i}{N} \left(\delta_{ij} + \rho_j G_{ij} \right)$$
 (2)

with

$$G_{ij} = 4\pi \int_0^\infty [g_{ij}(r) - 1] r^2 dr,$$
 (3)

as the standard definition for a Kirkwood-Buff integral. 40,43,44 In accordance with Refs. 43 and 44, Kirkwood-Buff integrals can be interpreted as excess volumes and can be further evaluated in order to estimate the excess number of particles $N_{ij}^{xs} = \rho_j G_{ij}$ such that Eq. (2) reads $S_{ij}(0) \approx (N_i/N)(\delta_{ij} + N_{ij}^{xs})$, which finally yields

$$N_{ij}^{xs} = \frac{N}{N_i} S_{ij}(0) - \delta_{ij} \tag{4}$$

as an appropriate expression for the excess number of particles in the simulation box. The last equation and Eq. (2) highlight the fact that the partial structure factor reveals a close relation with Kirkwood-Buff integrals⁴² such that peaks in S_{ij} can be ascribed to particle density fluctuations.

In order to study the dynamic behavior in the PIL system, one can calculate the particle mean-square displacement $\langle \Delta r_i^2(\tau) \rangle = \langle (\mathbf{R}_i(t_0 + \tau) - \mathbf{R}_i(t_0))^2 \rangle$, which can be inserted into the Einstein expression,

$$D_i = \lim_{\tau \to \infty} \frac{\langle \Delta r_i^2(\tau) \rangle}{6\tau},\tag{5}$$

for the calculation of the diffusion coefficient D_i with the position \mathbf{R}_i of a single particle in three spatial dimensions at long times $\tau \to \infty$. The introduction of the parameter β according to⁴⁵

$$\sqrt{\langle \Delta r_i^2(\tau) \rangle} \sim \tau^{\beta} + c_{\tau_0} \tag{6}$$

with the constant c_{τ_0} provides a meaningful distinction between different dynamic regimes. The presence of the diffusive regime, as indicated by $\beta=0.5$, dominates for long times according to the Einstein expression, whereas a value of $\beta<0.5$ can be observed at shorter times or for glass-like liquids 45,46 in the sub-diffusive regime. We ensured in all our simulations that $\beta=0.5$ holds for sufficiently long runs, which allows us to extract meaningful values for the ion transport numbers,

$$t^{\pm} = \frac{D_{\pm}}{D_{+} + D_{-}},\tag{7}$$

where D_{\pm} denotes diffusion coefficients of positively and negatively charged species, respectively, as introduced in Eq. (5).

A further important dynamic quantity to characterize ion transport is given by the ionic conductivity. Although equivalent expressions in terms of linear response relations with regard to particle velocities can be derived, ^{47,48} the

corresponding Einstein-Helfand relation for the ionic conductivity of charged species reads^{49,50}

$$\sigma_{\rm EH} = \lim_{\tau \to \infty} \frac{e^2}{6V\tau k_B T} \sum_{i,i} z_i z_j \langle \Delta \mathbf{r}_i(\tau) \Delta \mathbf{r}_j(\tau) \rangle, \tag{8}$$

which takes into account particle cross-correlations, whereas vanishing cross-correlations are expressed by the Nernst-Einstein approach in accordance with

$$\sigma_{\rm NE} = \lim_{\tau \to \infty} \frac{e^2}{6V\tau k_B T} \sum_i z_i^2 \langle \Delta r_i^2(\tau) \rangle, \tag{9}$$

which thus neglects ion-pairing effects.⁴⁹ The parameter e denotes the elementary charge, z_i the valency of particle i, T the temperature, and k_B the Boltzmann constant.

A challenging issue for simulations of polyelectrolytes arises with regard to the proper sampling of converged particle displacements and the onset of the diffusive regime. In order to overcome these limitations, we use an equivalent method for the calculation of the ionic conductivity with regard to the influence of an external electric field E_x in spatial x-direction. For sufficiently small values of the electric field E_x , such that the system remains in the linear-response regime, the corresponding expression for the ionic conductivity reads

$$\sigma_{\text{ion}} = \frac{e}{E_x} \left(z_+ \rho_+ \langle v_x^+ \rangle + z_- \rho_- \langle v_x^- \rangle \right), \tag{10}$$

with $\rho_{\pm} = N_{\pm}/V$ and mean anion and cation velocities $\langle v_x^{\pm} \rangle$ in x-direction. With regard to Eq. (10), it is also possible to evaluate a local ionic conductivity $\sigma_{\rm ion}(z)$ in z-direction by histogram techniques due to the consideration of local velocities $\langle v_x^{\pm}(z) \rangle$ and local particle number densities $\rho_{\pm}(z)$. It has to be noted that Eq. (10) is formally equivalent to Eq. (8) such that ion pairing effects are taken into account. Although we used a Langevin dynamics approach in our simulations, which is per construction not momentum-conserving, the electrostatic forces are much stronger than the random forces and reasonable results for the mobility of the species in the PIL system can be obtained.

III. COMPUTATIONAL DETAILS

As a main motivation concerning our PIL modeling approach, it should be noted that the objective of the coarse-graining procedure is primarily intended to map generic properties onto a simple bead-spring model. As reference for

our model, we choose the chemical structure of a popular imidazolium-based PIL, as shown in Fig. 1, with ILM building blocks including backbone groups and a cation group at terminal position in the side chain of varying particle number, here referred to as side chain length δ . With regard to the pronounced importance of the side chain in PILs, we thus use an extension, as schematically shown in Fig. 2, of existing simple bead-spring models. Furthermore, the positively charged beads are located at terminal position in the side chain, and counterions are explicitly modeled as negatively charged particles. All other particles including side chain and backbone beads are uncharged. With reference to the work by Limbach and Holm, ²⁶ the beads interact via a 12-6 Lennard-Jones (LJ) potential,

$$U_{\rm LJ}(r) = 4\epsilon_{\rm LJ} \left[\left(\frac{\sigma}{r} \right)^{12} - \left(\frac{\sigma}{r} \right)^{6} \right],\tag{11}$$

with the Lennard-Jones well-depth parameter $\epsilon_{LJ} = 1.75 k_B T$ and the particle or bead diameter σ . A cutoff radius of $r_{\rm cut}$ = 2.5 σ for the attractive part of the LJ potential is also introduced. The intention behind the introduction of attractive interactions can mainly be motivated by the occurrence of apolar clustering effects, as induced by alkylgroups of imidazolium-based cations in molecular ionic liquids.²³ The attractive part of the Lennard-Jones potential is neglected for all pair interactions between charged species. Recent simulation outcomes indicated the vanishing importance of dispersion interactions for anions like BF_4^- in molecular ionic liquids, which verifies this approach.⁵² Instead, for interactions with counterions, a shifted and truncated LJ-potential (WCA)⁵³ according to Eq. (11) is used, which vanishes for all distances $r \ge r_{\rm cut} = 2^{1/6} \sigma$. In order to study the influence of attractive interactions between the polymer beads, we also perform reference simulations where all attractive LJ interactions are truncated and thus represented by WCA interactions. The bonds between the polymer beads are modeled through FENE springs with the corresponding potential

$$U_{\text{FENE}}(\Delta b) = -\frac{1}{2} K \Delta b_{\text{max}}^2 \ln \left(1 - \left(\frac{\Delta b}{\Delta b_{\text{max}}} \right)^2 \right), \tag{12}$$

with actual bond length Δb , maximum stretching distance $\Delta b_{\text{max}} = 2 \sigma$, and spring constant $K = 7 \epsilon/\sigma^2$ with energy unit $\epsilon = k_B T$. As a mapping relation and with regard to the

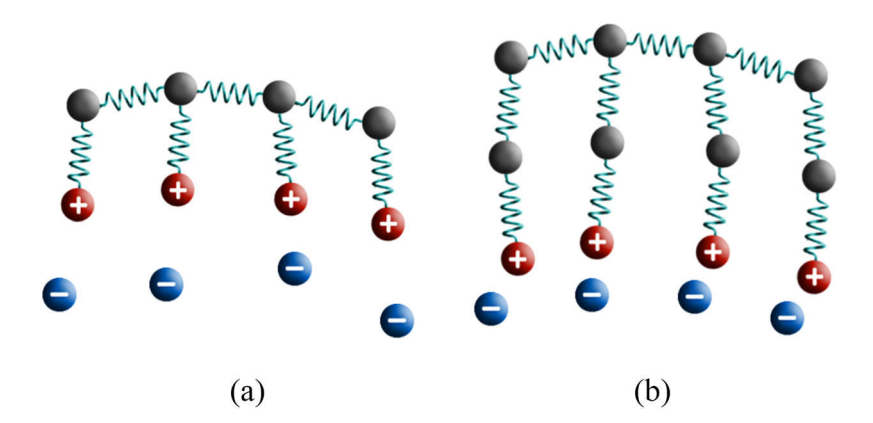


FIG. 2. Schematic illustration of the bead-spring model with N=4 monomers as an example for PILs with $\delta=1$ (a) and $\delta=2$ (b) side chain beads per monomer with terminal charged cation group (red) and mobile counterions (blue).

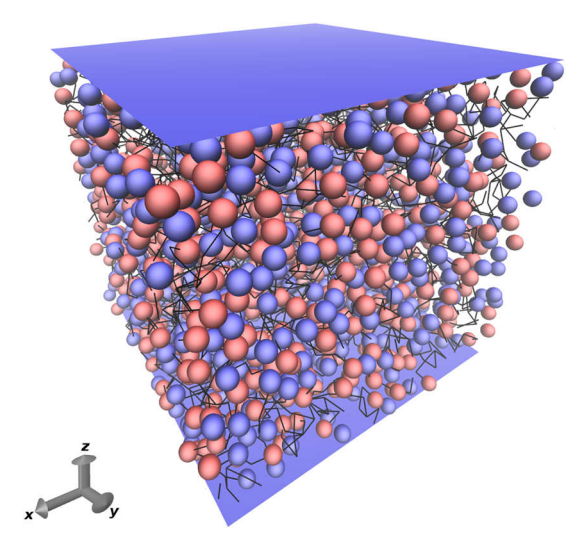


FIG. 3. Snapshot of a confined PIL system with $\delta=3$ between two infinitely extended walls at distinct z-positions. Uncharged particles are denoted by black lines, whereas counterions are drawn in blue and charged polymer beads in red color. The number of PIL chains is $N_p=30$ with a degree of polymerization $N_M=30$.

relatively low dielectric constant ϵ_r of the analogous room temperature ionic liquids and comparable PILs, ^{54,55} the Bjerrum length is set to $\lambda_B = e^2/(4\pi\epsilon_0\epsilon_r k_BT) = 7~\sigma$, which can be also evaluated in SI units according to $\lambda_B \approx 3.8$ nm for $\epsilon_r \approx 15$ as a reasonable assumption for PILs with the mapping relation $\sigma = 0.54$ nm according to the van-der-Waals volume of imidazolium ions, as discussed in the supplementary material of Ref. 8. Whereas the bulk PIL systems are simulated with full 3D periodic boundary conditions without spatial constraints, the confined systems include two uncharged and structureless walls at distinct z-positions in order to establish a 2D + h slit pore geometry as shown in Fig. 3. The walls interact via the above-mentioned WCA potential with all bead species and are thus purely repulsive.

All MD simulations are performed with ESPResSo.^{56,57} For full 3D periodic boundary conditions, the Coulomb interactions are calculated with the particle-particle particle-mesh (P³M) solver,^{58,59} which is combined with the electrostatic layer correction method in order to simulate confined PIL systems in slit pore geometries.^{60,61} We use a Langevin dynamics approach according to

$$m_i \ddot{\mathbf{R}}_i = -\zeta \dot{\mathbf{R}}_i + \boldsymbol{\eta}_i + \boldsymbol{F}_i \tag{13}$$

with the mass $m_i = 1$ m for all beads, the conservative forces F_i , and the friction coefficient $\zeta = 1.0 \ \sigma^{-1}(m\epsilon)^{1/2}$. The

random force η_i acts on each bead independently and obeys the fluctuation-dissipation theorem $\langle \eta_{ik} \rangle = 0$, and $\langle \eta_{ik}(t)\eta_{jl}(t') \rangle = 2\zeta k_B T \delta_{ij} \delta_{kl} \delta(t-t')$, which ensures the influence of Gaussian white noise for particles i and j in the spatial directions k and l. The temperature is set to $T = 2 \epsilon/k_B$, and the Langevin equation is integrated via a velocity Verlet algorithm with a time step of $\delta t = 0.01 \tau$ with $\tau = \sigma(m/\epsilon)^{1/2}$.

Motivated by the work of Zarubin and Bier for molecular ionic liquids⁶² in all simulations a constant particle packing fraction of

$$\theta = \frac{\pi}{6V} \sigma^3 N N_p \left(\delta + 2\right) = 0.3 \tag{14}$$

is used, with a number of chains $N_p = 30$ and a degree of polymerization $N_M = 30$. The actual cubic box length l for each PIL system with varying number of side chain beads $\delta \in \{0, 1, 2, 3\}$ is then fixed according to $l = V^{1/3}$.

The initial configurations of the different PIL systems are generated by slowly rescaling the particle coordinates to satisfy the fixed value of l for an initial box length of $l_s = 40~\sigma$ and further equilibration. The final box sizes for the individual systems are presented in the supplementary material. The equilibration run has a length of 7.5×10^5 MD steps representing $\tau_S = 7.5 \times 10^3~\tau$. For both the bulk and the confined PIL simulations, each production run is performed for at least 2×10^7 MD steps, according to a simulation time of $\tau_S = 2 \times 10^5~\tau$. In accordance with the work of Grass and Holm, 27 the external electric field value for the ionic conductivity calculations is chosen as $E_x = 0.05~\epsilon/(\sigma e)$ to ensure the validity of linear response relations.

IV. NUMERICAL RESULTS

A. Microphase separation in the bulk phase

We start the presentation of the results by the discussion of the structural properties in bulk PIL systems. Snapshots of the fully equilibrated PIL systems with varying side chain length are shown in Fig. 4. Uncharged beads are colored in red, while all charged beads and counterions are depicted in green color. It can be clearly seen that microphase separation occurs for larger side chain lengths with $\delta \geq 2$, as it becomes evident by the presence of red-colored domains. Thus, well-defined and connected apolar regions for $\delta = 3$ can be identified, whereas the occurrence of these regions vanishes with decreasing side chain length [Figs. 4(a) and 4(b)]. For shorter side chain lengths, one can indeed observe polar and hence charged regions in green color, which can be explained by the

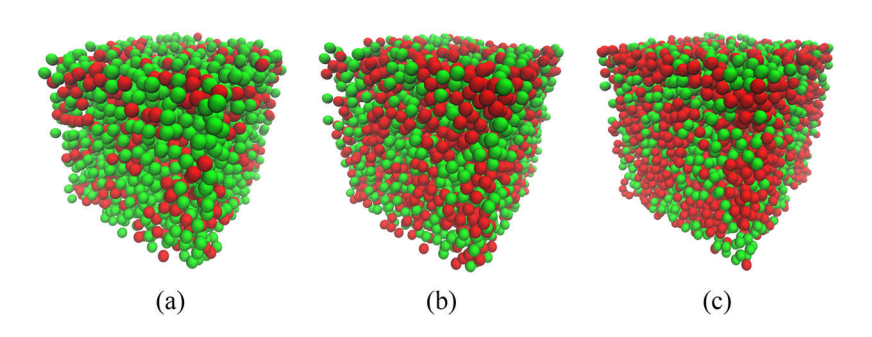


FIG. 4. Snapshots of PIL bulk systems with Lennard-Jones interactions with one (a), two (b), and three (c) side chain beads per ionic liquid monomer. Uncharged beads are colored in red, and charged beads including counterions are represented as green spheres. (a) $\delta = 1$, (b) $\delta = 2$, and (c) $\delta = 3$.

occurrence of pairs between counterions and charged terminal beads of PILs.

In order to study the corresponding microphase separation in more detail, we calculate the values for the partial structure factors according to Eq. (1) for the individual systems and between different combinations of species. Furthermore, we investigate the influence of attractive LJ interactions between the beads in comparison to repulsive WCA potentials. All results are calculated with regard to well-converged radial distribution functions (data shown in the supplementary material). The corresponding outcomes for varying side chain lengths in presence of LJ- and WCA-interactions are depicted in Figs. 5 and 6. In terms of attractive interactions (Fig. 5) and repulsive WCA interactions (Fig. 6), pronounced peaks at $q \approx 6.3 \ \sigma^{-1}$ corresponding to nearest

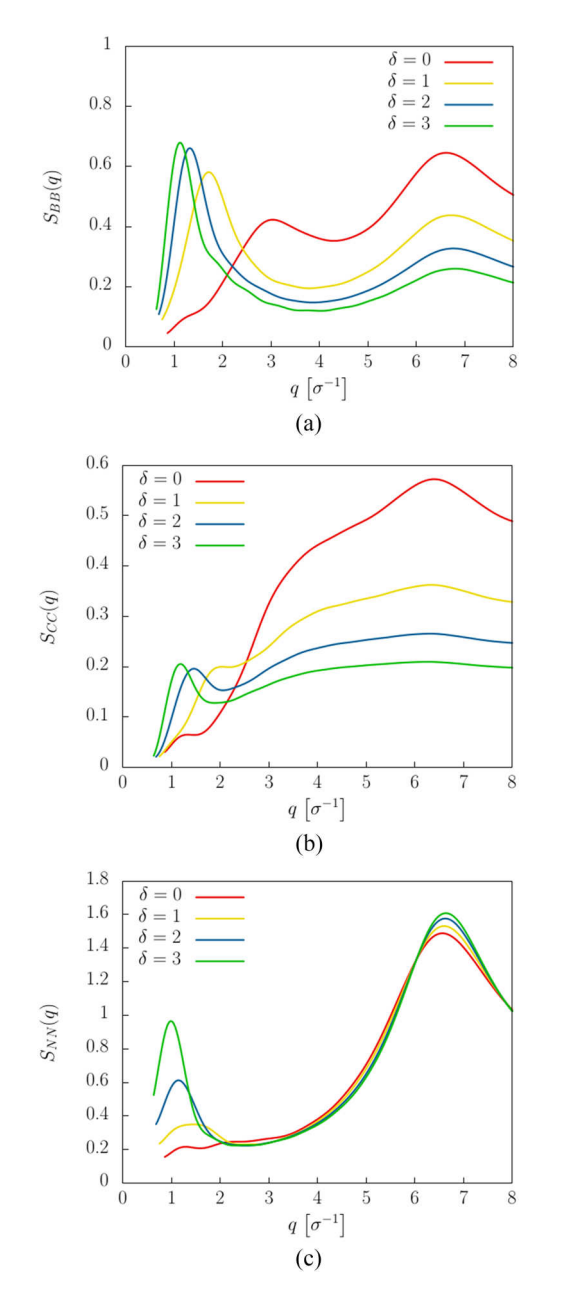


FIG. 5. Values of the partial structure factors for backbone-backbone beads S_{BB} (a), between counterions S_{CC} (b), and between all particles S_{NN} (c) for PIL bulk systems with attractive Lennard-Jones interactions.

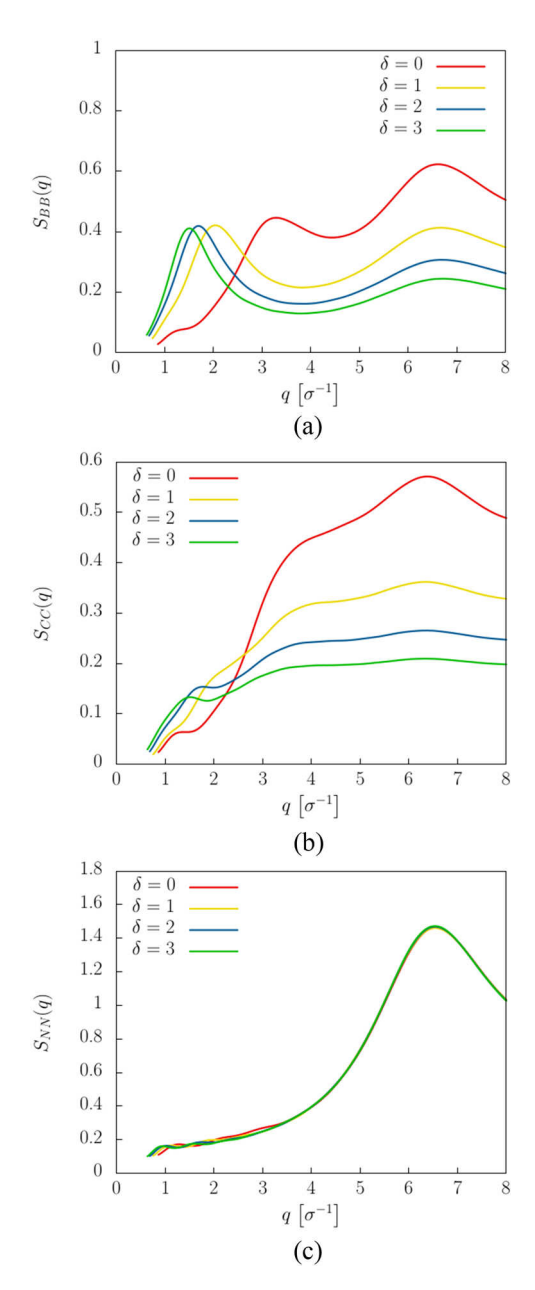


FIG. 6. Values of the partial structure factors for backbone-backbone beads S_{BB} (a), between counterions S_{CC} (b), and between all particles S_{NN} (c) for PIL bulk systems with repulsive WCA interactions.

neighbor interactions with $l_q = 2\pi/q \approx 1\sigma$ can be observed. In contrast to purely repulsive interactions, one can identify increasing peaks for increasing side chain lengths at regions $q = 0.9 \, \sigma^{-1} - 1.5 \, \sigma^{-1}$ for all studied structure factors with attractive interactions (Fig. 5). These wave numbers correspond to length scales $l_q \approx 4.2 \ \sigma - 7.0 \ \sigma$ and are thus long-ranged and a clear signature of microphase separation, as it was also discussed in Ref. 23 for molecular ionic liquids. The highest peak values in the partial structure factors can be observed for S_{BB} and thus for uncharged beads, which reveals the dominance of attractive LJ interactions. Furthermore, pronounced peaks in this region can also be observed in S_{NN} , which takes all particles into account. Hence, in agreement with experimental results,²⁰ it can be assumed that the corresponding length scales of the aforementioned microregions can be related to the average backbone-backbone distance.

The presence of microphase separation as induced by attractive interactions is also verified with regard to the corresponding results in presence of purely repulsive WCA interactions as depicted in Fig. 6. The presence of only small peak heights in Fig. 6 for S_{BB} and S_{CC} at $q < 2\sigma^{-1}$, when compared with Fig. 5 in presence of LJ interactions, implies a minor importance for the overall system behavior as reflected by S_{NN} and thus the absence of microphase separation effects for purely repulsive WCA interactions. Thus, all values for different side chain lengths clearly reveal an absence of pronounced peaks in S_{NN} . As a consequence, we can conclude that the presence of attractive interactions, or more precisely dispersion interactions, between uncharged beads is essential for the formation of apolar domains. Furthermore, longer side chains promote the accumulation of larger excess particle numbers [Eq. (4)] in these regions, which becomes evident by the increasing peak height values for increasing side chain lengths in Fig. 5. The absence of microphase separation for $\delta = 0$ can be simply explained by the fact that each bead in the PIL chain is charged such that only electrostatic interactions dominate in these

The positions $q_{\rm mp}$ of the main peak in the particle-particle structure factors S_{NN} are shown in Table I, which allow us to estimate the corresponding length scales of these regions via the relation $l_{mp} = 2\pi/q_{mp}$. In accordance with the values shown in Table I, one can observe an increase from $l_{\rm mp} = 4.3 \ \sigma \ {\rm for} \ \delta = 1 \ {\rm to} \ l_{\rm mp} = 6.35 \ \sigma \ {\rm for} \ \delta = 3.$ Hence, the actual size of the apolar regions increases with increasing side chain length. A comparable effect was observed for dialkylimidazolium-based molecular ionic liquids, where larger alkyl side chain lengths also stimulate the formation of microphases in terms of apolar clusters.²³ Moreover, our mapping relation $\sigma = 0.54$ nm thus provides SI values between $l_{\rm mp} = 2.3$ nm and $l_{\rm mp} = 3.4$ nm, which is a typical length scale for microphase separation in accordance with previous results for standard and novel ionomers and polyelectrolytes in different solvents. 63-65 As a consequence, we can relate the main driving force behind the formation of apolar domains to solvophobic effects in terms of unfavorable polar-apolar bead contact pairs.⁶⁶ Moreover, it can be clearly seen that all values of $S_{ii}(q)$ for $q \to 0$ are below 1, which reveals a deficit in the excess number of particles [cf. Eq. (4)]. In accordance with the relation $G_{ij} = N_{ii}^{xs}/\rho_j \ll 0$, it becomes, thus, evident that the system is dominated by excluded-volume effects at large scales. This behavior is a common principle for polymer solutions and can be often observed in coarse-grained simulations.

With regard to the dynamic properties, we calculated the anion and the cation transport numbers, respectively, for the PIL systems according to Eq. (7). The corresponding

TABLE I. Characteristic wave numbers $q_{\rm mp}$ and length scales $l_{\rm mp}$ for PILs with different side chain lengths δ as obtained from the values of S_{NN} in Fig. 5.

δ	$q_{ m mp}\left[\sigma^{-1} ight]$	$l_{ m mp}\left[\sigma ight]$	
1	1.46	4.30	
2	1.14	5.51	
3	0.99	6.35	

TABLE II. Anion diffusion coefficients D_- , ion transport numbers t^\pm , and corresponding ionic conductivities $\sigma_{\rm ion}$ according to Eq. (10) for PILs with different side chain lengths δ and WCA- or LJ-interactions, respectively. The errors for the diffusion coefficients and the ionic conductivities are of the order $\mathcal{O}(10^{-4})\sigma^2/\tau$.

Interaction type	δ	$D_{-}[\sigma^2/\tau]$	t^+	t^{-}	$\sigma_{\rm ion} \left[e^2/(\epsilon \sigma \tau) \right]$
LJ	0	0.20	0.02	0.98	5.26
LJ	1	0.19	0.04	0.96	2.75
LJ	2	0.19	0.04	0.96	1.93
LJ	3	0.20	0.05	0.95	1.47
WCA	0	0.19	0.02	0.98	4.94
WCA	1	0.18	0.03	0.97	2.40
WCA	2	0.18	0.04	0.96	1.64
WCA	3	0.17	0.05	0.95	1.17

results for PILs with LJ- and WCA-interactions are shown in Table II. Furthermore, we also calculated the ionic conductivity in presence of an external electric field according to Eq. (10). The results are also shown in Table II. All values for the anion transport numbers t^- reveal the overwhelming dominance of anion currents in PILs, which thus fulfill the requirements of single ion conductors. As a consequence, over 95% of the diffusional ionic transport is carried by the mobile counteranions in all systems, which can be mostly related to the low diffusivity of the PIL chains. These findings are also supported by the corresponding mean-square displacement behavior as shown in the supplementary material.

Moreover, it becomes evident that the values for the ratio between the ionic conductivities in presence of LJ- or WCA- interactions $\chi^{(\delta)} = \sigma_{\text{ion}}^{\text{LJ}}(\delta)/\sigma_{\text{ion}}^{\text{WCA}}(\delta)$ are constantly increasing with $\chi^{(0)} = 1.06$, $\chi^{(1)} = 1.14$, $\chi^{(2)} = 1.18$, and $\chi^{(3)} = 1.26$. Thus, it can be assumed that the formation of microphases, in terms of LJ interactions when compared with WCA interactions, induces a slightly higher relative ionic conductivity. As a consequence, the value for $\chi^{(0)}$, and thus in absence of microphases, is due to these reasons close to unity. Hence, we conclude that larger side chain lengths decrease the total conductivity, while the formation of apolar microphases slightly enhances the ionic transport. The general decrease of the ionic conductivity (Table II) can be rationalized by the resulting lower ion charge densities ρ_{\pm} for increasing side chain lengths in accordance with Eq. (10) due to fixed volume packing fractions in our simulations.

B. Ion conductivity channels in confined PIL systems

In order to study the influence of confinement on the PIL systems, we performed simulations in the presence of two uncharged, purely repulsive, parallel walls at distinct z-positions. The results for the probability distributions of charged species within the channel for different side chain lengths are depicted in Fig. 7. The different channel widths are adjusted to fulfill a constant particle packing fraction [Eq. (14)] in terms of increasing side chain lengths. It can be clearly seen that the presence of channel walls induces a local ordering effect, as reflected by increasing particle

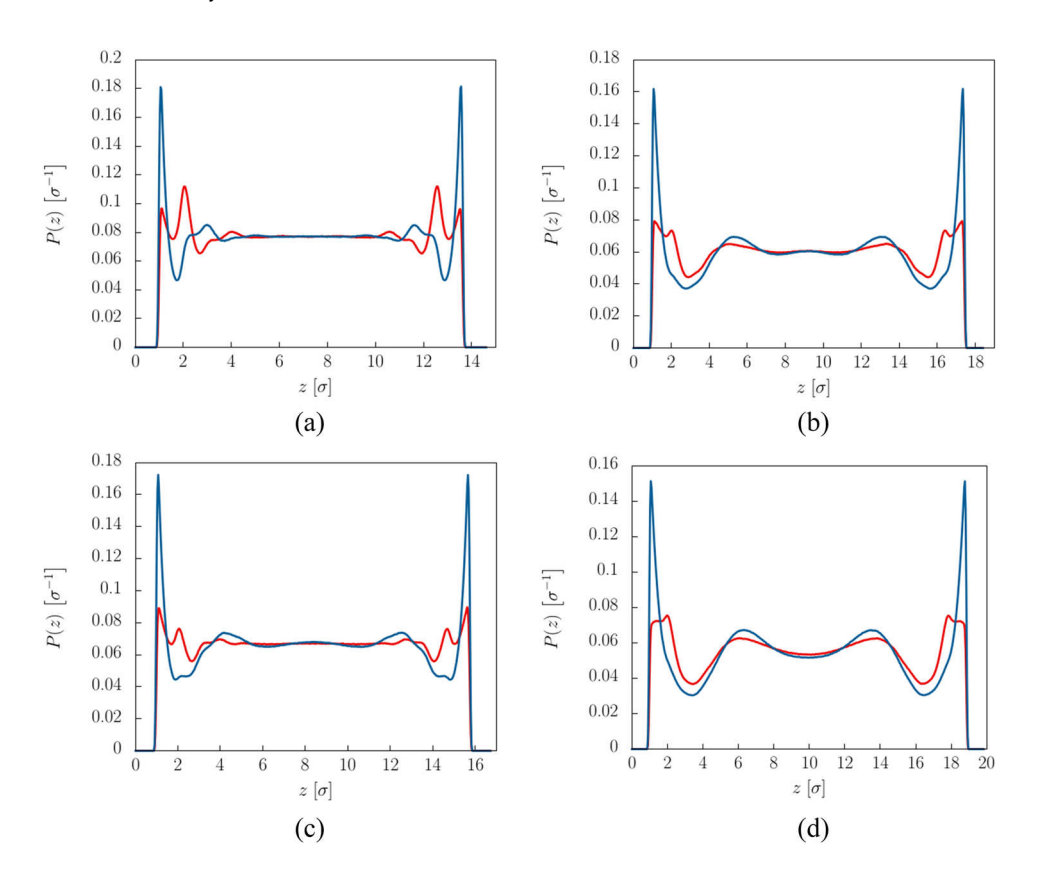


FIG. 7. Probability distributions P(z) for charged species and different PIL side chain lengths δ in the presence of electrically neutral and repulsive walls with WCA interactions. Charged polymer beads are drawn in red and counterion beads in blue. (a) $\delta = 0$, (b) $\delta = 1$, (c) $\delta = 2$, and (d) $\delta = 3$.

probabilities P(z) close to the boundaries. For $\delta=0$, we observe a layered structure of length $l_s=3.5~\sigma$ with regard to pronounced peaks in P(z) in close vicinity to the channel walls. The value of l_s increases with increasing δ from $l_s=6~\sigma$ ($\delta=1$) via $l_s=8~\sigma$ for $\delta=2$ to $l_s\gg8~\sigma$ for $\delta=3$. The latter value of l_s for the longest side chain length is only a rough estimate due to the absence of a well-defined bulk region within

the system. In more detail, one can observe an accumulation of counterions at the channel walls for all systems. Furthermore, also the existence of second-shell counterion peaks is evident, which are broadened and shifted to larger distances in the presence of longer side chains. Hence, the occurrence of well-defined counterion and PIL layers points to a complicated interplay between both species.

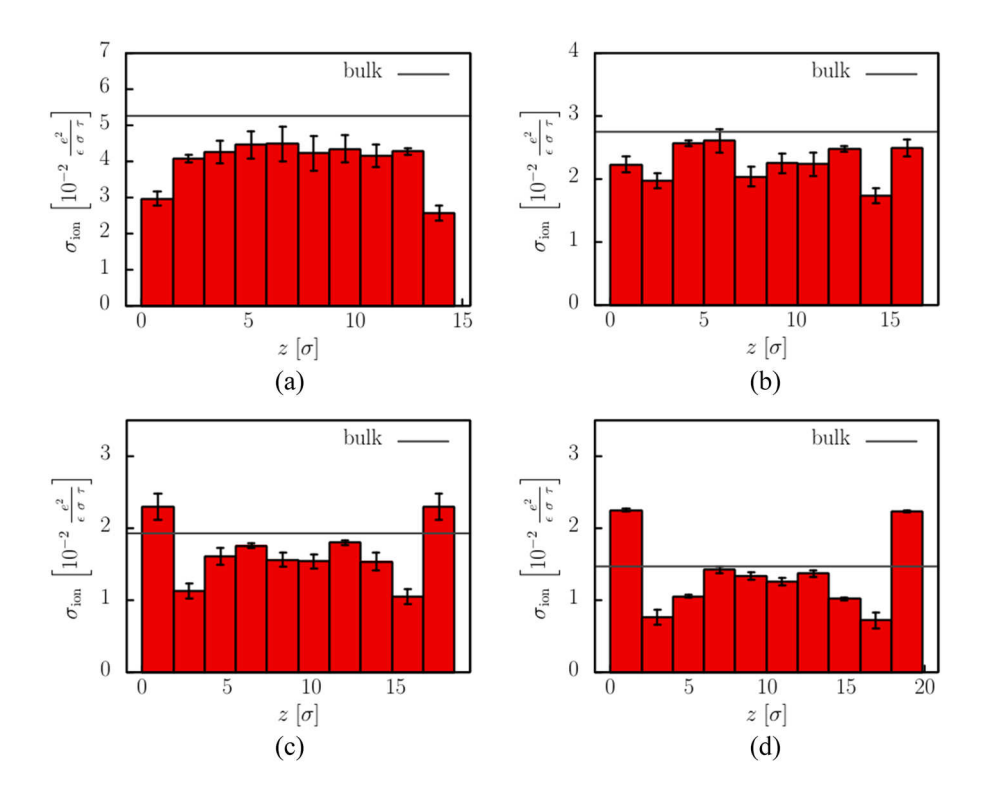


FIG. 8. Distribution of the ionic conductivities $\sigma_{\rm ion}(z)$ according to a local version of Eq. (10) for PIL systems with electrically neutral and repulsive walls, as calculated from the probability distributions and the stationary drift velocities of the charged species. The black solid lines represent the corresponding bulk ionic conductivities without confinement effects. (a) $\delta = 0$, (b) $\delta = 1$, (c) $\delta = 2$, and (d) $\delta = 3$.

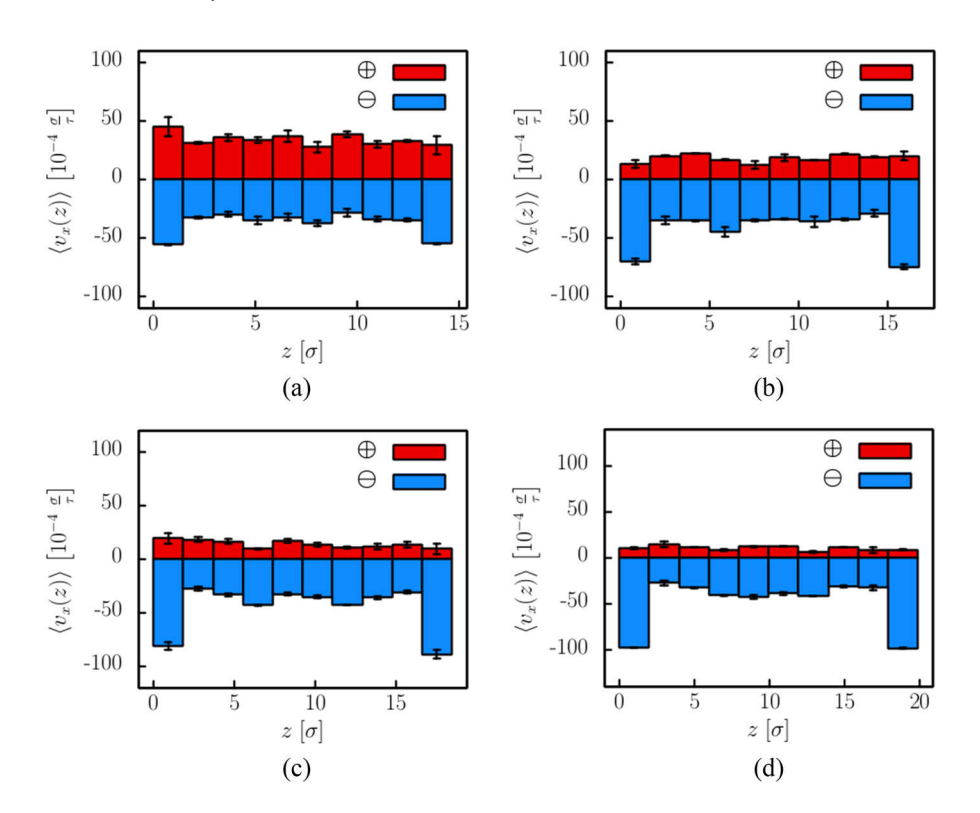


FIG. 9. Mean spatial drift velocities $\langle v_x(z) \rangle$ in the direction of the electric field for counterions (\oplus) and charged polymer beads (\oplus) and different PIL side chain lengths δ in the presence of electrically neutral and repulsive walls with WCA interactions. (a) $\delta = 0$, (b) $\delta = 1$, (c) $\delta = 2$, and (d) $\delta = 3$.

As a possible explanation, the high net charge at the channel walls, as a consequence of the pronounced counterion accumulation, enhances the electrostatic attraction of PIL chains. Based on this assumption, the first shell in front of the walls is indeed formed by counterions and to a smaller extent by charged PIL groups, whereas the second shell is predominantly formed by PIL beads. Notably, for PILs without side chains ($\delta = 0$), a pronounced and well-ordered layering effect for counterions and charged PIL beads occurs in accordance with the presence of two peaks. The pronounced peaks of P(z) slightly decrease and broaden for larger δ values due to the fact that the charged PIL chains with longer side groups reveal a higher orientational flexibility and thus promote a less strict ordering behavior.

Moreover, it has to be pointed out that the channel walls are uncharged. In consequence, any attractive interaction with the particles is absent, and it thus can be concluded that the resulting higher probability for the counterion distribution at the channel walls is solely driven by entropic contributions. Hence, the free space, which is not occupied by the PIL chains due to the chain-intrinsic restricted conformational behavior, is mostly filled by mobile counterions in order to increase the configurational entropy of the system. As a result, the formation of ion-rich regions at the boundaries is a generic effect, which does not depend on any enthalpic contributions from interactions with the channel walls. Nevertheless, it has to be mentioned, however, that the corresponding effects are slightly overestimated with regard to atomically flat surfaces and particle species with identical diameters in our systems.

The corresponding consequences on the ion transport behavior are shown in Fig. 8. In comparison to the total ionic conductivity in the bulk phase without confinement, it can be clearly seen that the corresponding mean ionic conductivity

is decreased in presence of walls. Furthermore, it turns out that increasing δ -values induce a relative increase of the ionic conductivity at the channel walls, which can be related to the counterion-rich regions in Fig. 7. Although the net value of the total ionic conductivity decreases, the local ionic conductivities are even larger than the bulk value for $\delta \geq 2$ in close vicinity to the channel walls. This effect can be explained by the corresponding slightly decreasing values of P(z) in Fig. 7 with increasing side chain length for charged PIL beads. As a consequence, the charge density is $\rho_{-}(z_B) \gg \rho_{+}(z_B)$ at distance $z_B = 1\sigma$ in front of the channel walls, and the corresponding charge density difference is highest for the largest side chain length δ . According to Eq. (10), this clearly induces the occurrence of large values concerning the local ionic conductivity $\sigma_{\text{ion}}(z_B)$ for PILs with side chain lengths $\delta \geq 2$. The corresponding results imply that ion conductivity channels mainly occur for branched polyelectrolytes with long side chains, which promotes their use in polymer-electrolyte membranes for electrochemical applications.

Furthermore, the results for the corresponding local mean drift velocities of the charged species in these regions (Fig. 9) reveal that this effect is mainly induced by differences in the corresponding local charge densities. In fact, the net mean velocity of counterions at the channel walls even increases with increasing values of δ such that the occurrence of counterionrich conductivity channels with high ionic conductivities is verified.

V. SUMMARY AND CONCLUSION

We performed coarse-grained MD simulations of poly(ionic liquid)s and their counterions in bulk solution and under confinement. A specific focus was set on the influence of

varying side chain lengths δ with terminal charge groups. The partial structure factors reveal the formation of apolar domains for longer side chains in bulk PIL systems. We observed a monotonic increase of domain size for increasing δ -values. A significant influence on the formation of these regions arises from the presence of attractive Lennard-Jones interactions, mimicking dispersion interactions between uncharged, apolar groups. In contrast, for purely repulsive WCA interactions, the formation of these domains is suppressed. With regard to the values for the ionic conductivities according to repulsive and attractive interactions, we observed a relative increase for the ratio of the conductivities in presence of attractive LJ interactions. The beneficial use of PILs as single ion conducting materials⁶⁷ was also verified by our results for the counterion transport numbers, which exhibit values close to unity. Thus, charge transport in PIL systems can be mostly attributed to mobile counterions due to the low mobility of PIL chains.

Furthermore, our simulations indicate the formation of ion conductivity channels under confinement. For larger side chain lengths, we observed an increasing ionic conductivity in close vicinity to the channel walls. This finding can be mainly attributed to the corresponding pronounced structural order behavior in PIL systems near the boundaries. Due to the absence of attractive interactions between the particles and the channel walls considered here, we can conclude that the occurrence of these highly ordered regions is solely induced by entropic contributions. These findings point to far-reaching implications for technological applications. In fact, increasing the local ionic conductivity is beneficial for the use in electrochemical devices and can be simply achieved by the presence of obstacles or additives such as colloidal objects. Due to the fact that this effect is of entropic nature, it should in principle be observable for all polyelectrolytes with long side chains including charged terminal groups in combination with small counterions. In fact, previous experimental results^{20–22} point to sophisticated PIL architectures such that it can be assumed that the drawback of low total ionic conductivities for larger side chains can be circumvented by a well-defined synthesis of PILs, which leaves room for the formation of optimized ion conductivity channels as a generic effect. Furthermore, it may be important to study the orientational behavior of PILs in more detail and in particular in front of charged interfaces. For instance, recent publications⁶⁸⁻⁷¹ reported on differences between nematic and smectic phases for molecular ILs with regard to varying side chain lengths, which may be also relevant for PIL systems. In summary, we verified the existence of novel ion transport behavior and structural order effects in confined and bulk PIL systems. Our findings can be of technological interest in order to promote the further application of PILs, e.g., in modern electrochemical devices.

SUPPLEMENTARY MATERIAL

See supplementary material for more results on the meansquare displacement of species, radial distribution functions, and detailed information on the system geometries.

ACKNOWLEDGMENTS

The authors thank Volker Lesch, Diddo Diddens, Falk Frenzel, Jiayin Yuan, Frank Uhlig, and Johannes Zeman for useful hints and valuable discussions. Financial funding is gratefully acknowledged from the Deutsche Forschungsgemeinschaft through the cluster of excellence initiative Simulation Technology (EXC 310).

- ¹D. Mecerreyes, Prog. Polym. Sci. **36**, 1629 (2011).
- ²H. Ohno and K. Ito, Chem. Lett. **27**, 751 (1998).
- ³J. Yuan and M. Antonietti, Polymer **52**, 1469 (2011).
- ⁴J. Yuan, D. Mecerreyes, and M. Antonietti, Prog. Polym. Sci. 38, 1009
- ⁵W. Qian, J. Texter, and F. Yan, Chem. Soc. Rev. **46**, 1124 (2017).
- ⁶J. Tang, H. Tang, W. Sun, M. Radosz, and Y. Shen, J. Polym. Sci. A 43, 5477 (2005).
- ⁷E. I. Privalova, E. Karjalainen, M. Nurmi, P. Mäki-Arvela, K. Eränen, H. Tenhu, D. Y. Murzin, and J.-P. Mikkola, ChemSusChem 6, 1500 (2013).
- ⁸P. Li, D. Paul, and T.-S. Chung, Green Chem. **14**, 1052 (2012). ⁹M. Sadeghpour, R. Yusoff, and M. K. Aroua, Rev. Chem. Eng. 33, 183
- ¹⁰Q. Zhao, J. W. Dunlop, X. Qiu, F. Huang, Z. Zhang, J. Heyda, J. Dzubiella, M. Antonietti, and J. Yuan, Nat. Commun. 5, 4293 (2014).
- ¹¹Q. Zhao, J. Heyda, J. Dzubiella, K. Täuber, J. W. Dunlop, and J. Yuan, Adv. Mater. 27, 2913 (2015).
- ¹²O. Green, S. Grubjesic, S. Lee, and M. A. Firestone, Polym. Rev. 49, 339 (2009)
- ¹³R. Marcilla, F. Alcaide, H. Sardon, J. A. Pomposo, C. Pozo-Gonzalo, and D. Mecerreyes, Electrochem. Commun. 8, 482 (2006).
- ¹⁴T. Y. Kim, H. W. Lee, M. Stoller, D. R. Dreyer, C. W. Bielawski, R. S. Ruoff, and K. S. Suh, ACS Nano 5, 436 (2011).
- ¹⁵H. Ohno, Electrochim. Acta **46**, 1407 (2001).
- ¹⁶Y. Ye and Y. A. Elabd, Macromolecules **44**, 8494 (2011).
- ¹⁷Y. Ye and Y. A. Elabd, Polymer **52**, 1309 (2011).
- ¹⁸H. Chen, J.-H. Choi, D. Salas-de la Cruz, K. I. Winey, and Y. A. Elabd, Macromolecules 42, 4809 (2009).
- ¹⁹M. Lee, U. H. Choi, R. H. Colby, and H. W. Gibson, Chem. Mater. 22, 5814 (2010).
- $^{20}\mathrm{D}.$ Salas-de la Cruz, M. D. Green, Y. Ye, Y. A. Elabd, T. E. Long, and K. I. Winey, J. Polym. Sci., Part B: Polym. Phys. 50, 338 (2012).
- ²¹U. H. Choi, Y. Ye, D. Salas de la Cruz, W. Liu, K. I. Winey, Y. A. Elabd, J. Runt, and R. H. Colby, Macromolecules 47, 777 (2014).
- ²²U. H. Choi, A. Mittal, T. L. Price, M. Lee, H. W. Gibson, J. Runt, and R. H. Colby, Electrochim. Acta 175, 55 (2015).
- ²³J. N. Canongia Lopes and A. A. Pádua, J. Phys. Chem. B **110**, 3330 (2006).
- ²⁴W. Jiang, Y. Wang, and G. A. Voth, J. Phys. Chem. B **111**, 4812 (2007).
- ²⁵S. Mogurampelly, J. R. Keith, and V. Ganesan, J. Am. Chem. Soc. 139, 9511 (2017).
- ²⁶H. J. Limbach and C. Holm, J. Phys. Chem. B **107**, 8041 (2003).
- ²⁷K. Grass and C. Holm, Soft Matter **5**, 2079 (2009).
- ²⁸J. Smiatek and F. Schmid, J. Phys. Chem. B **114**, 6266 (2010).
- ²⁹J. Smiatek and F. Schmid, Comput. Phys. Commun. **182**, 1941 (2011).
- ³⁰F. Fahrenberger, O. A. Hickey, J. Smiatek, and C. Holm, Phys. Rev. Lett. 115, 118301 (2015).
- ³¹L. M. Hall, M. J. Stevens, and A. L. Frischknecht, Macromolecules **45**, 8097 (2012).
- ³²C. L. Ting, M. J. Stevens, and A. L. Frischknecht, Macromolecules **48**, 809
- ³³D. Roy and M. Maroncelli, J. Phys. Chem. B **116**, 5951 (2012).
- ³⁴K. Breitsprecher, P. Košovan, and C. Holm, J. Phys.: Condens. Matter 26, 284108 (2014).
- ³⁵K. Breitsprecher, P. Košovan, and C. Holm, J. Phys.: Condens. Matter 26, 284114 (2014)
- ³⁶R. Burt, K. Breitsprecher, B. Daffos, P.-L. Taberna, P. Simon, G. Birkett, X. Zhao, C. Holm, and M. Salanne, J. Phys. Chem. Lett. 7, 4015 (2016).
- ³⁷L. Leibler, Macromolecules **13**, 1602 (1980).
- ³⁸Y. Ye, J.-H. Choi, K. I. Winey, and Y. A. Elabd, Macromolecules **45**, 7027 (2012).
- ³⁹C. Willa, J. Yuan, M. Niederberger, and D. Koziej, Adv. Funct. Mater. 25, 2537 (2015).
- ⁴⁰T. Kobayashi, J. E. S. J. Reid, S. Shimizu, M. Fyta, and J. Smiatek, Phys. Chem. Chem. Phys. 19, 18924 (2017).

- ⁴¹J.-P. Hansen and I. R. McDonald, *Theory of Simple Liquids* (Elsevier, 1990).
- ⁴²J. W. Nichols, S. G. Moore, and D. R. Wheeler, Phys. Rev. E **80**, 051203 (2009).
- ⁴³J. G. Kirkwood and F. P. Buff, J. Chem. Phys. **19**, 774 (1951).
- ⁴⁴A. Ben-Naim, Statistical Thermodynamics for Chemists and Biochemists (Springer Science & Business Media, 2013).
- ⁴⁵B. Doliwa and A. Heuer, Phys. Rev. Lett. **80**, 4915 (1998).
- ⁴⁶V. Lesch, A. Heuer, C. Holm, and J. Smiatek, Phys. Chem. Chem. Phys. 17, 8480 (2015).
- ⁴⁷C. Schröder and O. Steinhauser, J. Chem. Phys. **131**, 114504 (2009).
- ⁴⁸A. N. Krishnamoorthy, J. Zeman, C. Holm, and J. Smiatek, Phys. Chem. Chem. Phys. **18**, 31312 (2016).
- ⁴⁹H. K. Kashyap, H. V. Annapureddy, F. O. Raineri, and C. J. Margulis, J. Phys. Chem. B 115, 13212 (2011).
- ⁵⁰V. Lesch, S. Jeremias, A. Moretti, S. Passerini, A. Heuer, and O. Borodin, J. Phys. Chem. B 118, 7367 (2014).
- ⁵¹M. Doi and S. F. Edwards, *The Theory of Polymer Dynamics* (Oxford Science Publications, 1986).
- ⁵²V. Lesch, A. Heuer, C. Holm, and J. Smiatek, ChemPhysChem 17, 387 (2016).
- ⁵³J. D. Weeks, D. Chandler, and H. C. Andersen, J. Chem. Phys. **54**, 5237 (1971).
- ⁵⁴T. Singh and A. Kumar, J. Phys. Chem. B **112**, 12968 (2008).
- ⁵⁵ U. H. Choi, A. Mittal, T. L. Price, Jr., H. W. Gibson, J. Runt, and R. H. Colby, Macromolecules 46, 1175 (2013).
- ⁵⁶H. J. Limbach, A. Arnold, B. A. Mann, and C. Holm, Comput. Phys. Commun. **174**, 704 (2006).

- ⁵⁷A. Arnold, O. Lenz, S. Kesselheim, R. Weeber, F. Fahrenberger, D. Röhm, P. Košovan, and C. Holm, *Meshfree Methods for Partial Differential Equations VI*, Lecture Notes in Computational Science and Engineering Vol. 89, edited by M. Griebel and M. A. Schweitzer (Springer, Berlin Heidelberg, 2013), pp. 1–23.
- ⁵⁸ A. Arnold and C. Holm, *Advanced Computer Simulation Approaches for Soft Matter Sciences II*, Advances Polymer Science Vol. II, edited by C. Holm and K. Kremer (Springer, Berlin, 2005), pp. 59–109.
- ⁵⁹A. Arnold, F. Fahrenberger, C. Holm, O. Lenz, M. Bolten, H. Dachsel, R. Halver, I. Kabadshow, F. Gähler, F. Heber, J. Iseringhausen, M. Hofmann, M. Pippig, D. Potts, and G. Sutmann, Phys. Rev. E 88, 063308 (2013).
- ⁶⁰A. Arnold, J. de Joannis, and C. Holm, J. Chem. Phys. **117**, 2496 (2002).
- ⁶¹J. de Joannis, A. Arnold, and C. Holm, J. Chem. Phys. **117**, 2503 (2002).
- ⁶²G. Zarubin and M. Bier, J. Chem. Phys. **142**, 184502 (2015).
- ⁶³A. Wohlfarth, J. Smiatek, K.-D. Kreuer, S. Takamuku, P. Jannasch, and J. Maier, Macromolecules 48, 1134 (2015).
- ⁶⁴K.-D. Kreuer, A. Wohlfarth, C. C. de Araujo, A. Fuchs, and J. Maier, ChemPhysChem 12, 2558 (2011).
- ⁶⁵B. P. Grady, Polym. Eng. Sci. **48**, 1029 (2008).
- ⁶⁶J. Smiatek, A. Wohlfarth, and C. Holm, New J. Phys. **16**, 025001 (2014).
- ⁶⁷S. Dou, S. Zhang, R. J. Klein, J. Runt, and R. H. Colby, Chem. Mater. 18, 4288 (2006).
- ⁶⁸W. Li, J. Zhang, B. Li, M. Zhang, and L. Wu, Chem. Commun. 35, 5269 (2009).
- ⁶⁹S. Kondrat, M. Bier, and L. Harnau, J. Chem. Phys. **132**, 184901 (2010).
- ⁷⁰ A. Pană, I. Pasuk, M. Micutz, and V. Cîrcu, CrystEngComm **18**, 5066 (2016).
- ⁷¹A. Alvarez Fernandez and P. H. Kouwer, Int. J. Mol. Sci. 17, 731 (2016).